UNIVERSITY OF LEEDS

This is a repository copy of *Fabrication of magnetic and photocatalytic polyamide fabric coated with Fe2O3 particles*.

White Rose Research Online URL for this paper:
http://eprints.whiterose.ac.uk/86306/

Version: Accepted Version

Article:
Zhang, H, Liu, Y and Mao, N (2015) Fabrication of magnetic and photocatalytic polyamide fabric coated with Fe2O3 particles. Fibers and Polymers, 16 (2). 10.1007/s12221-015-0378-1. pp. 378-387. ISSN 1229-9197

https://doi.org/10.1007/s12221-015-0378-1

(c) 2015, The Korean Fiber Society and Springer Science+Business Media Dordrecht. This is an author produced version of a paper published in Fibers and Polymers. Uploaded in accordance with the publisher's self-archiving policy. The final publication is available at Springer via http://dx.doi.org/10.1007/s12221-015-0378-1

Reuse
Unless indicated otherwise, fulltext items are protected by copyright with all rights reserved. The copyright exception in section 29 of the Copyright, Designs and Patents Act 1988 allows the making of a single copy solely for the purpose of non-commercial research or private study within the limits of fair dealing. The publisher or other rights-holder may allow further reproduction and re-use of this version - refer to the White Rose Research Online record for this item. Where records identify the publisher as the copyright holder, users can verify any specific terms of use on the publisher's website.

Takedown
If you consider content in White Rose Research Online to be in breach of UK law, please notify us by emailing eprints@whiterose.ac.uk including the URL of the record and the reason for the withdrawal request.

White Rose university consortium
Universities of Leeds, Sheffield & York

eprints@whiterose.ac.uk
https://eprints.whiterose.ac.uk/

Fabrication of Magnetic and Photocatalytic Polyamide Fabric Coated with Fe_2O_3 Particles

Hui Zhang[*1], Yulin Liu[1] and Ningtao Mao[1,2]

[1]School of Textile & Materials, Xi′an Polytechnic University, Xi′an 710048, China

[2]School of Design, University of Leeds, Leeds, LS2 9JT, United Kingdom

[*] Corresponding author: Hui Zhang, School of Textile & Materials, Xi′an Polytechnic University, Xi'an City, Shaanxi Province, China

E-mail: hzhangw532@xpu.edu.cn; hzhangw532@163.com

Phone: 0086 029 13002929736

Fax: 0086 029 82330365

Abstract

Hematite (alpha-Fe_2O_3) particles are prepared and synchronously deposited on the surface of polyamide (PA) fabric using ferric sulfate as the precursor, sodium hydroxide as the precipitant, and sodium dodecyl benzene sulfonate as the dispersant in a low temperature hydrothermal process. The Fe_2O_3 coated PA fabric is then modified with silane coupling agent Z-6040. The Fe_2O_3 coated PA fabric and remaining particles are systematically characterized by different techniques, such as small-spot Micro X-ray Fluorescence (μ-XRF), field-emission scanning electron microscopy (FESEM), energy dispersive X-ray spectroscopy (EDX), transmission electron microscopy (TEM), X-ray diffraction (XRD), Fourier transform infrared spectroscopy (FTIR), X-ray photoelectron spectroscopy (XPS), thermal gravimetric analysis (TGA), differential scanning calorimetry (DSC), diffuse reflectance spectrum (DRS), and vibrating sample magnetometer (VSM). The properties of tensile, durable washing and photocatalytic activity are investigated. The experimental results show that Fe_2O_3 particles composed of nanoparticles having the average crystallite size of 37.8 nm are grafted onto PA fabric and enhanced by coupling agent via the C-Fe, O-Fe and Si-O-Fe bonds. It is found that, after treatments, the thermal stability of PA fabric hardly changes; the visible light absorption capability and magnetism are gained; and the tensile property decreases slightly. It is also confirmed that the Fe_2O_3 coated PA fabric can withstand the repeated washings up to 20 times and photodegrade the adsorbed methyl orange (MO) exposed to ultraviolet (UV) irradiation. Therefore, the present method provides a new strategy for the production of durable magnetic fabric.

Keywords: Polyamide (PA) fabric, hematite Fe_2O_3, hydrothermal

Introduction

Hematite (alpha-Fe_2O_3) as an n-type semiconductor has an antiferromagnetic nature with a band gap of 2.3 eV under ambient conditions and it can effectively photocatalyze a number of chemical reactions [1]. However, the applications of the iron oxides depend on the particle geometry and morphology, particle size and particle size distribution and surface chemistry. It has been shown that the presence of the porous surface and smaller crystallite size in the alpha-Fe_2O_3 nanostructures can significantly enhance the photocatalytic degradation of organic dyes [2]. Also, the visible photocatalytic activities of alpha-Fe_2O_3 nanocomposites have been greatly promoted by coupling with N-doped graphene [3]. Likely, the magnetic properties might be controlled by modulating the particle size and the alignment of the Fe_2O_3 nanoparticles in the matrix by applying an external magnetic filed [4].

The particle shape, size and surface chemistry of the alpha-Fe_2O_3 nanoparticle is related to the variables of its synthesis routes, and the composition, crystallinity, grain growth, and morphologies of alpha-Fe_2O_3 nanostructures can be selectively synthesized by hydrothermal and solvothermal procedures [5]. With different processing parameters including precursor concentration, pH value, reaction temperature, reaction time and type of surfactant in hydrothermal process, the size and morphology of alpha-Fe_2O_3 are controllable. The examples of different morphologies of alpha-Fe_2O_3 nanostructures obtained include 1D nanorods [6] and nanoribbons [7], nanodisk [8], 3D structures including microspheres [9, 10], truncated nanooctahedra [11], almond-shaped [12], polyhedron-shaped nanoparticles [13, 14], rhombohedral [15], and quasi-cubes [16], as well as dendrites and hierarchical nanostructures such as snowflakes [17], peanuts-like, capsule-like, cantaloupe-like, urchin-like [18], pod-like [19], platelet-like [20], flower-like [21] nanoparticles. It has been proved that the resultant alpha-Fe_2O_3 particles are of different optical, magnetic, electrochemical, and photocatalytic properties [22, 23].

Textile materials loaded with magnetic nanoparticles have been made for diverse applications [24]. For

example, Fe_2O_3 microtubules have been synthesized via sol-gel [25] and supercritical carbon dioxide [26] routes using cellulose fiber as the template. It is indicated that the coercivity of the resultant microtubules decreases with the addition of surfactant and increases after the samples are calcinated [27]. Monodisperse alpha-Fe_2O_3 nanostructures are also prepared in an efficient Bombyx mori silk fibroin assisted hydrothermal process, and the morphologies of alpha-Fe_2O_3 nanostructures having shape-dependent magnetic properties are greatly influenced by the concentration of the silk fibroin [28]. Multi-functional polyester (PET) fabrics having magnetic, antibacterial and sono-Fenton catalytic properties are fabricated in situ synthesis of Fe_3O_4 and alpha-Fe_2O_3 nanoparticles using ferric chloride, ferrous sulfate and sodium hydroxide at various temperatures [29].

In previous paper, we reported an alpha-Fe_2O_3 coated PET fabric obtained via a facile hydrothermal route [30]. While PET fabrics, which is acidic resistant but prone to alkali solution, are excellent fibrous support substrates for the alpha-Fe_2O_3 nanoparticles, it thus might not be suitable for the applications in alkali environments. Polyamide (PA) fabric is one of the most commonly used textile materials having best abrasion resistance and is widely utilized for clothes fabrics, package paper, carpets and ropes, and thus should also be an excellent fibrous support substrates for alpha-Fe_2O_3 nanoparticle and the alpha-Fe_2O_3 coated PA fabrics are expected to have potential applications in medical, electronic, and catalytic fields. However, PA fabrics are alkali resistant and prone to acidic solution and thus might not stand the acidic hydrothermal process for making the alpha-Fe_2O_3 nanoparticles; thus little research is found related to magnetic PA fabric deposited with the alpha-Fe_2O_3 nanoparticles.

In this study, in order to impart the PA fabric with the photocatalytic and magnetic properties, alpha-Fe_2O_3 nanoparticles are synthesized and simultaneously immobilized on the surface of PA fabric by using ferric sulfate and sodium hydroxide in a hydrothermal process. The resultant Fe_2O_3 coated PA fabric is further modified with the silane coupling agent Z-6040. X-ray diffraction (XRD), transmission electron microscopy

(TEM), and vibrating sample magnetometer (VSM) analysis are carried out to characterize the alpha-Fe_2O_3 nanoparticles synthesized. Comparisons are made between the structure and properties of the uncoated and alpha-Fe_2O_3 coated PA fabrics by using several techniques including field-emission scanning electron microscopy (FESEM), energy-dispersive X-ray (EDX), Fourier transform infrared spectroscopy (FTIR), X-ray photoelectron spectroscopy (XPS), thermal gravimetric analysis (TGA), differential scanning calorimetry (DSC), and diffuse reflectance spectrum (DRS). Finally, the properties of tensile, attachment and photocatalytic activity are assessed.

Experiments

Materials

An undyed polyamide (PA) fabric with plain weave structure, which was obtained from Haiyan Jiaxia Chemical Fiber Co. Ltd, was used as the support substrates for the deposition of Fe_2O_3 particles. The linear mass densities of yarns are 8 tex for both warp and weft yarns. The numbers of threads per 10 centimeter of the fabric in both warp and weft directions are 420 and 300 respectively. Reagent grade chemicals including ferric sulfate ($Fe_2(SO_4)_3$, Tianjin Bodi Chemical Co., Ltd), sodium hydroxide (NaOH, Tianjin Kemel Chemical Reagent Co., Ltd), sodium dodecyl benzene sulfonate (SDBS, $C_{18}H_{29}NaO_3S$, Shanghai Aibi Chemicals Preparation Co., Ltd), N,N-dimethylformamide (DMF, $HCON(CH_3)_2$, Shanghai Aibi Chemicals Preparation Co., Ltd), acetone (C_3H_6O, Nanchang Lanxiang Chemical Co., Ltd), anhydrous ethanol (C_2H_6O, Nanchang Lanxiang Chemical Co., Ltd) and methyl orange (MO, $C_{14}H_{14}N_3NaO_3S$, Shenzhen Xinhua Chemical Tech Co., Ltd), were used without further purification. Deionized water was applied for the fabrication processes. The silane coupling agent Z-6040 (γ-glycidoxypropyltrimethoxysilane, $(CH_3O)_3Si(CH_2)_3OCH_2CH\text{-}CH_2$) was provided by Dow Corning (Shanghai) Co., Ltd.

Deposition of Fe_2O_3 Particles on the PA Fabrics

About 0.8 g of PA fabric was firstly soaked in 80 ml of 6% hydrochloric acid solution at 60°C for 30 minutes. After being washed with deionized water, it was immersed in 30 ml of N,N-dimethylfomamide solution at 80°C for 3 hours, and then was successively washed twice with acetone, anhydrous ethanol and deionized water. The hydrothermal method was used for the deposition of Fe_2O_3 particles on the PA fabric. A certain amounts of ferric sulfate (0.03 mol/l) and sodium hydroxide (0.18 mol/l) were dissolved into 40 ml of deionized water at 40°C and magnetically stirred for 10 minutes. About 0.1 g of SDBS was subsequently added into the above suspension under vigorous stirring. The pretreated PA fabric was accordingly submerged into the suspension for 3 minutes. The suspension containing the fabric was transferred to a 50 ml PTFE-lined stainless steel autoclave. Six identical autoclaves were simultaneously prepared according to the above method, which was placed in a furnace for the hydrothermal treatment. The autoclave was heated to 110°C at a speed of 1°C/min. After 4 hours, the autoclave was cooled down to the room temperature naturally. The Fe_2O_3 coated PA fabric was taken out and dipped in the anhydrous ethanol solution for 5 min without stirring. The remaining particles were separated from the solution by centrifugation, and then repeatedly washed with acetone, anhydrous ethanol and deionized water, respectively, and dried in a vacuum oven at 80°C for 12 h.

Modification of Fe_2O_3 coated PA Fabric

About 2 ml of silane coupling agent Z-6040 was dripped into 40 ml of anhydrous ethanol under vigorous stirring and 60 ml of deionized water was then added to dilute the solution at the room temperature. The Fe_2O_3 coated PA fabric was immediately immersed into the above mixture at 60°C under magnetic stirring. After 4 hours, the fabric sample was put under the Philips ultraviolet (UV) lamp at a distance of 10 cm. The main wavelength of the UV irradiation is 365 nm and the power is 40 W. After exposure to irradiation for 30 min on each side, the fabric sample was dried at 80°C for 30 min, and then mildly cured at 120°C for 3 min. The

modified Fe_2O_3 coated PA fabric was dipped in acetone, anhydrous ethanol and deionized water for 10min, respectively, and finally dried at 80°C in vacuum air.

Characterization and Measurement

The information on composition and 2D element distribution of the modified Fe_2O_3coated PA fabric was measured using the M4 TORNADO small-spot Micro X-ray Fluorescence (μ-XRF) analysis system.

The surface morphologies of PA fabric before and after treatments were further observed using a JEOL JSM-6700 field emission scanning electron microscope (FESEM). The elemental analysis was also conducted on an Oxford INCA Energy 400 energy-dispersive X-ray (EDX) spectrometer in the FESEM.

The microstructure of the remaining particles was determined by transmission electron microscopy (TEM, JEOL3010, 200 keV).

The X-ray diffraction (XRD) diffractogram of the remaining particles was obtained by using a 7000S diffractometer. It used a monochromatized Cu $_{K\alpha1}$ radiation (λ=0.154056 nm) at 40 kV and 40 mA and a graphite monochromator in the 2θ range of 10–80° at a scan speed of 8 deg/min. The crystallite size of the particles was calculated using Scherrer equation $D=K\lambda/\beta cos\theta$ (where D is the diameter of the particle, λ is the X-ray wavelength, β is the FWHM of the diffraction line, θ is the diffraction angle, and K is a constant 0.89).

The Fourier transformed infrared (FTIR) spectra of the fabric and particle samples were obtained using a FT-IR 7600 spectrophotometer (Lambda Scientific Systems, Inc). The samples were mixed with potassium bromide to obtain a uniform pellet. The spectra were in the range 400–4000 cm^{-1} at a resolution of 4 cm^{-1}.

The surface chemical compositions and bonding states of PA fabric before and after treatments were characterized by an X-ray photoelectron spectroscope (XPS) using a Thermo Scientific Kα X-ray photoelectron spectrometer. The samples were analyzed using a monochromatic Al Kα radiation at a binding energy of 1486.68 eV as the X-ray source. The vacuum of the analysis chamber was less than 8×10^{-6} Pa. All

binding energies were calibrated to the $_{C1s}$ peak at 284.6 eV. The XPS peak areas and peak decomposition were studied by using the Thermo Scientific Avantage Data System. The spectrum was first smoothed by using the Savitsky-Golay algorithm (auto-apply changes). The peak background was then processed by using the smart algorithm. The peak was fitted by using the Gaussian-Lorentzian mixed algorithm.

The thermogravimetric (TG) and differential scanning calorimetry (DSC) measurements were performed in a NETZSCH STA 449F3 instrument at a constant heating rate of 10 K/min with a nitrogen flush rate of 20 ml/min over the range of 40–550°C. The onset, endset and peak decomposition temperatures were evaluated using the NETZSCH Proteus Thermal Analysis Software Version 5.1.

The diffuse reflectance spectrum (DRS) of the fabric sample in the 200–800 nm wavebands was recorded using a U-3010 UV-VIS-NIR spectrometer with an integrated sphere attachment using $BaSO_4$ as the reference at a scanning speed of 120 nm/min. The change of the reflectance was calculated by subtracting the reflectance value of the modified Fe_2O_3 coated fabric sample from the reflectance value of the untreated one at corresponding wavebands in DRS spectra.

The static magnetic properties of the as-prepared fabric and particles were assessed using a vibrating sample magnetometer (VSM, Quantum Design Corp.) at a temperature of 300 K. The sample placed at the holder was caused to vibrate vertically at a frequency of 40 Hz and amplitude of 2 mm. The coercivity and remnant magnetization were obtained by the intercepts in the horizontal and longitudinal coordinates in the magnetic hysteresis loops, respectively.

The tensile properties of the fabric sample were measured using a YG(B)026D-500 electromechanical test instrument according to GB/T3923.1-1997. The initial gauge length was 200 mm and the width was 50 mm. The testing rate was 100 mm/min and the pretension was 2 N.

To evaluate the bonding strength between Fe_2O_3 particles and PA fabric, about 0.5 g of the fabric sample was mixed with 200 ml deionized water at 40^{o}C and 0.2 g commercial detergent (AATCC 1993 standard

detergent without optical brightener) was added into the suspension. The fabric sample was washed under magnetically stirring for 20 min, and subsequently soaked in anhydrous ethanol at 40°C for 10 min and then rinsed with deionized water at ambient temperature for 15 min, and dried in an oven at 80°C for 30 min. After 20 washing cycles, the fabric sample was observed by the above mentioned FESEM.

The photocatalytic activity of the fabric sample was carried out by the photo-decolorization of MO at room temperature under UV lights. About 0.25 g of the fabric sample was immersed in 50 ml of 2 mg/l MO aqueous solution. After 6 h in the dark to reach the adsorption and desorption equilibrium, the reaction solution was irradiated by a Philips 20 W UV lamp with a main wavelength of 254 nm at a distance of 10 cm. The absorbance at 464 nm was monitored using a UV-1600 spectrophotometer (Beijing Rayleigh Analytical Instrument Corp.) every other hour. The degradation rate D was expressed as follows: $D=(1-A_t/A_0)\times 100\%$. Where A_0 was the initial absorbance of MO solution which reached absorption equilibrium, and A_t was the absorbance of MO solution at time t. The standard curve between the concentration and the absorbance for MO solution was calibrated based on the Beer-Lambert's law. The apparent photo-decolorization rate constant k of MO solution was calculated according to a first order kinetic equation: $\ln(C_0/C) = f(t) = kt$, where C_0 is the initial concentration of MO aqueous solution, C is the concentration of MO solution at time t [31]. The MO solution was replaced with fresh solution and the reusability of the modified Fe_2O_3 coated PA fabric sample was measured based on the above method.

Results and Discussion

μ-XRF Analysis

The chemical composition identification and homogeneity analysis of the modified Fe_2O_3 coated PA fabric are shown in Figure 1. It is seen from the optical photograph that the finally obtained PA fabric is uniformly stained by the reddish-brown color. Also, the elements of Fe, Si, Al, S and K are homogeneously distributed in

the examined area. In comparison with Si, Al, S and K elements, the element of Fe becomes more intense.

The results of elemental analysis are listed in the Supporting Information S1 (see Table S1). It is obvious that the major elements are Fe (72.78%) and Si (23.90%), along with minor components of Al (2.61%), S (0.29%) and K (0.42%). Therefore, the PA fabric is evenly deposited with a layer of iron oxide particles.

FESEM and EDX Analyses

The microstructure and elemental analysis of PA fabric before and after treatments are measured by means of FESEM and EDX, as illustrated in Figure 2. It is observed that the surface of the untreated PA fiber is smooth and clean without any substances [Fig. 2(a)]. The EDX results confirm that the chemical compositions of the untreated PA fabric are constituted of C, O, and N elements [Fig. 2(b)]. In contrast, the surface of the modified Fe_2O_3coated PA fiber is homogeneously coated with a layer of aggregation substances [Fig. 2(c)]. The resultant EDX analysis is in agreement with the components of iron oxide and silane coupling agent. Besides C, N and O, the elements of Fe and Si are detected [Fig. 2(d)]. The agglomerated material consists of smaller spherical particles with a narrow distribution of shapes and dimensions. These micrometer-sized aggregates of the nanoparticles are closely embedded into the substrate of PA fiber [Fig. 2(e)]. From the high-magnification FESEM image of the modified Fe_2O_3 coated PA fabric [Fig. 2(f)], the sizes of the submicron-sized particles are in the range of 300~500 nm in diameter.

TEM Analysis

The TEM and HRTEM micrographs and selected area electron diffraction (SAED) pattern of the remaining particles are depicted in the Supporting Information S2 (see Figure S2). The representative TEM micrograph of the remaining particles indicates that the particles have the tetrahedral or quasi-spherical shape [Fig. S2(a)]. Obviously, the size of the particle remaining in the solution is larger than that adhered onto fiber surface. Thus, the growth or agglomeration of as-synthesized particles loaded on fabric surface is effectively inhibited during the same hydrothermal condition. The high-resolution TEM micrograph clearly shows the resolved

lattice fringes with interplanar spacing of 0.37 nm, which is in accord with the (012) crystal plane (0.368 nm) of alpha-Fe_2O_3 [32]. The optical transparent edge of the particle is attributed to the organic matter [Fig. S2(b)]. The bright diffraction spots of the SAED pattern reveal that the Fe_2O_3 particles are single-crystalline [Fig. S2(c)].

XRD Analysis

The XRD diffractogram of the remaining particles is represented in Figure 3. As shown, a series of diffraction peaks are noticed at 2θ=24.2°, 33.2°, 35.6°, 40.8°, 49.4°, 54.0°, 57.5°, 62.4°, 64.0°, 71.9° and 75.4°, which are identical to the (012), (104), (110), (113), (024), (116), (018), (214), (300), (1,0,10) and (220) crystal planes of hematite with a rhombohedral corundum structure. These characteristic peaks are consistent with the data list in JCPDS Card No.33-0664 [33]. The crystallite size of Fe_2O_3 particles is estimated by measuring the full width at half maximum (FWHM) of (104), (110) and (116) reflections based on Scherrer's equation. The average crystallite size is calculated to be 37.8 nm, which is far smaller than that observed from the TEM micrograph.

FTIR Analysis

The FTIR spectra of PA fabric before and after treatments and Fe_2O_3 particles are exhibited in Figure 4. It is clear that the spectrum of the modified Fe_2O_3 coated PA fabric is almost similar to the spectrum of the untreated one. After treatment, the strong peak centered at 3424 cm^{-1} is reduced to 3400 cm^{-1}, which corresponds to the absorption bands of O-H stretching mode of OH groups and N-H stretching mode of NH groups. This is due to the surface absorbed-water induced by Fe_2O_3 particles. The peaks at 1639 (C=O stretching) and 689 (N-H out-of-plane bending) cm^{-1} are shifted to 1645 and 692 cm^{-1}, respectively. That is ascribed to the hydrolysis of PA fiber. In comparison with the FTIR spectrum of Fe_2O_3 particles, the peak at 569 cm^{-1} associated to the stretching vibration of the Fe-O functional groups is not found in the modified Fe_2O_3 coated PA fabric [34]. One reason is that the Fe-O band is overlapped with the out-of-plane deformation vibration of C=O of PA fiber. The other

reason is that the Fe_2O_3 particles deposited on PA fabric is of little amount, which is beyond the IR detection limitation. Moreover, the absorption bands of the coupling agent are not identified because of the very small amount of Z-6040. It is proposed that the methoxy groups of Z-6040 are first hydrolyzed to produce active silanol groups to form polysiloxanes. The polysiloxanes then hydrogenate with OH groups of Fe_2O_3 particles. The covalent linkages eventually form with Fe_2O_3 coated PA fabric after UV curing [35]. As a result, it is difficult to judge whether the Fe_2O_3 particles are grafted onto PA fabric.

XPS Analysis

The survey scan and high-resolution core level XPS spectra of the bonding partners (C_{1s}, O_{1s}, N_{1s}, Si_{2p} and Fe_{2p}) for PA fabric before and after treatments are presented in the Supporting Information S3 (see Figure S3). The quantitative elemental analysis results are summarized in the Supporting Information S4 (see Table S1). It is evident that the elements of silicon (101.97 eV) and iron (710.28 eV) are detected in the Fe_2O_3 coated PA fabric [Fig. S3(a)]. The $_{C1s}$ core level spectra for the untreated PA fabric are fitted into four sub-peaks with binding energies of 284.59, 285.97, 287.56 and 288.60 eV, which are assigned to C-C, C-N, C=O and O-C=O, respectively [36]. After treatment, two new sub-peaks at 283.41 (C-Fe) and 286.64 (C-O) eV in the $_{C1s}$ core level spectra of the modified Fe_2O_3 coated PA fabric are observed [Fig. S3(b) and S3(c)] [37].

In comparison with the $_{O1s}$ XPS spectra of untreated PA fabric, the sub-peak of aliphatic -OH at 533.05 eV disappears, which is associated to the absorbed oxygen induced by pretreatment. The sub-peaks at 530.84 (O=C-O) and 531.85 (O=C) eV increase to 532.22 and 533.59 eV, respectively [38]. Meanwhile, four new sub-peaks at binding energies of 528.80, 529.80, 531.10 and 535.27 eV are observed [Fig. S3(d) and S3(e)]. The sub-peak at 528.80 eV is ascribed to O atoms of PA fabric bound to Fe of Fe_2O_3 [39]. The sub-peak at 529.80 eV is attributed to O atoms bound to Fe of Fe_2O_3particles [40]. The sub-peaks at 531.10 and 535.27 eV are correlated to the O-Si and O-C functional groups, respectively [41].

Besides the sub-peak at binding energy of 398.50 eV (N-C), a new sub-peak at 400.17 eV (N-H) is noted for the modified Fe_2O_3 coated PA fabric [Fig. S3(f) and S3(g)]. The $_{Si2p}$ XPS spectrum can be deconvoluted into four distinct sub-peaks [Fig. S3(h)]. The sub-peaks at 100.35, 101.54, 102.38 and 103.80 eV represent the Si-O-Si, Si-O-H, Si-O-C and Si-O-Fe groups, respectively [42].

The $_{Fe2p}$ core level peaks are split into eight sub-peaks [Fig. S3(i)]. The sub-peak appeared at binding energy of 709.65 eV is attributed to the $Fe^{3+}{}_{2p3/2}$ and another one localized at 722.73 eV corresponds to the $Fe^{3+}{}_{2p1/2}$ of Fe_2O_3. The slitting between $Fe^{3+}{}_{2p1/2}$ and $Fe^{3+}{}_{2p3/2}$ core levels is 13.08 eV, which is consistent with the normal state of Fe^{3+} in the hematite [33]. The sub-peaks at 712.43 and 725.61 eV are related to Fe atoms of Fe_2O_3 bound to O of PA fabric, respectively. The sub-peaks at 715.57 and 729.14 eV correspond to Fe atoms of Fe_2O_3 bound to C of PA fabric. The sub-peaks at 718.84 and 732.81 eV are ascribed to Fe atoms of Fe_2O_3 bound to Si-O of coupling agent, respectively. So it is demonstrated in the above results that the Fe_2O_3 particles are grafted on the surface of PA fabric via the C-Fe, O-Fe and Si-O-Fe bonds.

TG and DSC Analyses

The TG and DSC curves of PA fabric before and after treatments are compared in Figure 5. It is apparent from TG curves [Fig. 5(a)] that the onset decomposition temperature slightly increases from 410.6°C to 412.7°C after PA fabric is treated with ferric sulfate and sodium hydroxide and then modified with Z-6040. The corresponding endset decomposition temperature hardly changed (455.3°C vs. 454.5°C). In addition, the weight loss decreases from 94.31% to 88.76% over the full temperature range. Accordingly, the amount of Fe_2O_3 particles deposited on PA fabric is estimated about 5.55%, which is very close to the measured value of 5.4%. It is obvious from DSC curves [Fig. 5(b)] that in comparison with the untreated PA fabric, the endothermic peak of the Fe_2O_3-coated PA fabric slightly decreases from 223.4°C to 220.0°C. The corresponding major endothermic peak decreases from 444.3°C to 440.2°C. This is due to the coating of Fe_2O_3 particles. Hence, the thermal stability of PA fabric changes hardly changes even if it is subjected to the hot

pressure water and chemicals under hydrothermal conditions.

DRS Analysis

The diffuse reflectance spectra of PA fabric before and after treatments are displayed in Figure 6. It is worth noting that the untreated PA fabric has the capability of absorbing UV irradiation. The dominant absorption region from 200 to 350 nm is attributed to the characteristic structure of PA. After treatment, the reflectance decreases distinctly in UV region and the absorption edge extends to visible region (550 nm), implying the Fe_2O_3 coated PA fabric has a good photocatalytic activity. The average reflectances for the Fe_2O_3-coated PA fabric are reduced from 18.8% to 5.0% in UVB waveband and from 43.9% to 5.3% in UVA waveband in comparison with the untreated PA fabrics, respectively. At the same time, the average reflectance decreases by 72% in visible region. Based on the linear fit and the abscissa, the band-gap of the Fe_2O_3 coated PA fabric is estimated around 2.3 eV [43], irrespective of the substrate. This is very well correlated with the value (1.9–2.3 eV) reported for the band gaps of Fe_2O_3 [44].

VSM analysis

The magnetic hysteresis loops of the modified Fe_2O_3 coated PA fabric and Fe_2O_3 particles at 300 K are collected in Figure 7. It is observed that, as the applied magnetic field increases, the magnetization of the Fe_2O_3 particles increases progressively. The saturation of magnetization as a function of the field is not observed up to the maximum applied magnetic field of 30000 Oe, which is in accordance with the result of previous work [21]. The linear increase in the magnetization is ascribed to the contribution of the Fe_2O_3 antiferromagnetic core. The magnetization of the as-prepared Fe_2O_3 particles is smaller than that in previous studies [29], as this is influenced by the microstructural characteristics of the crystal structure [45]. The coercivity and remnant magnetization of Fe_2O_3 particles are calculated to be 292 Oe and 0.077 emu/g respectively (see inset of Fig. 7), indicative of soft magnets induced by surface spin disorder and shape anisotropy [46]. For the modified Fe_2O_3 coated PA fabric, the magnetization decreases significantly in

comparison with the Fe_2O_3 particles. The coercivity is estimated to be 205 Oe and the remnant magnetization is reduced to 0.0072 emu/g.

Tensile Property

The volumetric densities and tensile properties of PA fabric before and after treatments are given in the Supporting Information S5 (see Table S2) according to GB/T3923.1-1997. Because the coated fabric shrunk during its hydrothermal treatment at high temperature for a great time duration, the fabric densities in both warp and weft directions increase. The shrinkages of the modified Fe_2O_3 coated PA fabric are calculated about 9.2% in warp direction and 9.0% in weft direction, respectively. After treatment, the breakage strength and breakage elongation in both directions increase to some extent, which are mainly ascribed to the increase of the fabric densities. Thus the hydrothermal treatment has some influence on the mechanical properties of PA fabric.

Durable Washing

The surface morphology and EDX spectrum of the modified Fe_2O_3 coated PA fabric after being washed for 20 cycles are shown in the Supporting Information S6 (see Figure S4). It is seen from the FESEM image that many small aggregates are still anchored on the surface of the modified Fe_2O_3 coated PA fabric after it is subjected to 20 washing cycles. While it is demonstrated in the EDX results that the chemical elements of C, N, O, Si and Fe still remain in the fabric, the amount of element Fe decreases from 44.87% to 37.15% by mass percentage and from 17.39% to 12.86% by atomic percentage, respectively. Therefore, it is concluded that the bonding strength between Fe_2O_3 particles and PA fabric is strong enough to withstand repeated washings.

Photocatalysis

The effect of irradiation time on the degradation rate of MO solution exposed to UV irradiation is depicted in Figure 8. It is clear that the degradation rate increases with the increases of irradiation time for all coated

fabrics. The MO dye was able to be photodegraded to a lesser extent under UV light [47]. The untreated PA fabric can absorb MO dye to some degree. After 8h of UV irradiation, the degradation rates are around 19% for the MO solution without any fabric, 27% for the untreated PA fabric and 95% for the modified Fe_2O_3-coated fabric, respectively. The enhancement of the photodegradation of MO dyes for the modified Fe_2O_3-coated PA fabric is attributed to the photocatalytic activity of Fe_3O_3 particles [48]. The photodegradation of MO follows approximately a first order kinetic model [49]. The apparent rate constants are 0.196 min^{-1} for Fe_2O_3 coated PA fabric and 0.038 min^{-1} for untreated PA fabric, larger than 0.017 min^{-1} for the MO solution without PA fabric. The corresponding squared correlation coefficients (R^2) are larger than 0.98 for all samples. The results show that after 5 cycles of UV irradiation, the degradation rate for the modified Fe_2O_3 coated fabric is less than 85%. This is because the active sites on fabric surface are reduced to some degree because of the increased retardation effect, which result in the decrease of competitive adsorption of OH^- species and a lower formation rate of OH· radical [31]. Therefore, the degradation rate of MO dye decreases as the degradation cycle increases.

Conclusions

In this study, a layer of hematite Fe_2O_3 particles are deposited on the surface of PA fabric homogeneously to make the fabric have magnetic and photocatalytic properties by means of low temperature hydrothermal method. The results from FESEM, μ-XRF, and XRD examinations indicate that submicron-sized hematite Fe_2O_3 particles are aggregates of nano-scaled Fe_2O_3 particles with average crystal size of 37.8 nm. It is also illustrated in the results from both FTIR and XPS that Fe_2O_3 particles interact with PA fabric via the C-Fe, O-Fe and Si-O-Fe chemical bonds. In comparison with the characteristics in both TG and DSC for untreated PA fabric, the thermal stability of the Fe_2O_3 coated PA fabric hardly changes. It is confirmed in DRS, VSM, durable washing and photocatalysis experiments that the Fe_2O_3 coated PA fabric modified with coupling

agents has the ability to absorb UV irradiation, respond to applied magnetic field, resist to washing and photodegrade organic dye. The tensile properties of the Fe_2O_3 coated fabric largely are retained. The magnetic and photocatalytic properties of this Fe_2O_3 coated PA fabric could be particularly attractive for the various applications in textiles, electronics, medicine, military products.

Acknowledgement

This work has been supported by the Innovation Fund of Postgraduate (No. chx2013007) of Xi'an Polytechnic University. The corresponding author also acknowledges the Youth Leading Scholar Supporting Plan of Xi'an Polytechnic University.

References

1. Z. Zhang, M. F. Hossain, and T. Takahashi, Appl. Catal. B-Environ., **95,** 423 (2010).
2. J. Sundaramurthy, P. S. Kumar, M. Kalaivani, V. Thavasi, S. G. Mhaisalkar, and S. Ramakrishna, RSC. Adv., **2,** 8201 (2012).
3. L. M. He, L. Q. Jing, Y. B. Luan, L. Wang, and H. G. Fu, ACS. Catal., **4,** 990 (2014).
4. S. L. Liu, R. Li, J. P. Zhou, and L. N. Zhang, Carbohyd. Polym., **87,** 830 (2012).
5. N. Thanh-Dinh, Nanoscale., **5,** 9455 (2013).
6. H. G. Cha, S. J. Kim, K. J. Lee, M. H. Jung, and Y. S. Kang, J. Phys. Chem. C., **115,** 19129 (2011).
7. D. Sarkar, M. Mandal, and K. Mandal, ACS. Appl. Mater. Inter., **5,** 11995 (2013).
8. W. Han, J. G. Deng, S. H. Xie, H. G. Yang, H. X. Dai, and C. T. Au, Ind. Een. Chem. Res., **53,** 3486 (2014).
9. J. S. Xu and Y. J. Zhu, Crystengcomm., **14,** 2702 (2012).
10. L. Xu, J. X. Xia, K. Wang, L. G. Wang, H. M. Li, H. Xu, L. Y. Huang, and M. Q. He, Dalton. T., **42,**

6468 (2013).

11. S. Yang, Y. Y. Xu, Y. Q. Sun, G. Y. Zhang, and D. Z. Gao, Crystengcomm., **14,** 7915 (2012).

12. X. H. Zhang, Y. Z. Chen, H. Liu, Y. Wei, and W. Wei, J. Alloy Compd., **555,** 74 (2013).

13. M. Khalil, J. J. Yu, N. Liu, and R. L. Lee, J. Nanopart. Res., **16,** 2362 (2014).

14. Z. F. Dou, G. P. Wan, L. F. Bao, and C. Y. Cao, J. Nanosci. Nanotechno., **14,** 5587 (2014).

15. Z. Liu, B. L. Lv, D. Wu, Y. H. Sun, and Y. Xu, Particuology., **11,** 327 (2013).

16. X. Zhou, C. Wang, W. Feng, P. Sun, X. W. Li, and G. Y. Lu, Mater. Lett., **120,** 5 (2014).

17. S. Bharathi, D. Nataraj, M. Seetha, D. Mangalaraj, N. Ponpandian, Y. Masuda, K. Senthil, and K. Yong, Crystengcomm., **12,** 373 (2010).

18. S. Y. Zeng, K. B. Tang, T. W. Li, and Z. H. Liang, J. Phys. Chem. C., **114,** 274 (2010).

19. W. C. Zhu, X. L. Cui, L. Wang, T. Liu, and Q. Zhang, Mater. Lett., **65,** 1003 (2011).

20. J. Liang, L. Li, W. M. Song, J. Z. Fang, M. Luo, and Y. P. Li, Cryst. Res. Technol., **45,** 405 (2010).

21. Q. Zhang, X. W. Lu, L. Y. Chen, Y. X. Shi, T. Xu, and M. L. Liu, Mater. Lett., **106,** 447 (2013).

22. H. Li, Z. Lu, Q. Li, M. H. So, C. M. Che, and R. Chen, Chem-Asian. J., **6,** 2320 (2011).

23. M. Y. Zhu, Y. Wang, D. H. Meng, X. Z. Qin, and G. W. Diao, J. Phys. Chem. C., **116,** 16276 (2012).

24. S. L. Liu, D. D. Tao, and L. N. Zhang, Powder. Technol., **217,** 502 (2012).

25. Q. L. Li and C. R. Zhang, J. Ceram. Process. Res., **11,** 331 (2010).

26. S. J. Xu, D. P. Shen, and P. Y. Wu, J. Nanopart. Res., **15,** 1557 (2013).

27. C. B. Chang, C. R. Zhang, W. Y. Wang, and Q. L. Li, Rare. Metals., **29,** 501 (2010).

28. X. Fei, Z. Z. Shao, and X. Chen, J. Mater. Chem. B., **1,** 213 (2013).

29. T. Harifi and M. Montazer, J. Mater. Chem. B.. **2,** 272 (2014).

30. H. Zhang, J. Song, and C. K. Liu, Ind. Eeg. Chem. Res., **52,** 7403 (2013).

31. P. Sharma, R. Kumar, S. Chauhan, D. Singh, and M. S. Chauhan, J. Nanosci. Nanotechno., **14,** 6153

(2014).

32. M. Tadic, N. Citakovic, M. Panjan, Z. Stojanovic, D. Markovic, and V. Spasojevic, J. Alloy. Compd., **509,** 7639 (2011).

33. O. Akhavan and R. Azimiradb, Appl. Catal. A-Gen., **369,** 77 (2009).

34. J. Y. Kim, J. S. Kim, and M. Y. Lee, Surf. Coat. Tech., **205,** 372 (2010).

35. S. Aoyama, K. Sumiya, and M. Amemiya, J. Mater. Sci., **23,** 1729 (1998).

36. R. Bessada, G. Silva, M. C. Paiva, and A. V. Machado, Appl. Surf. Sci., **257**, 7944 (2011).

37. S. Y. Liu, J. Xie, Q. Pan, C. Y. Wu, G. S. Cao, T. J. Zhu, and X. B. Zhao, Int J. Electrochem. Sci., **7,** 354 (2012).

38. M. J. Ariza, J. Benavente, E. Rodriguez-Castellon, and L. Palacio, J. Colloid Interf. Sci., **247,** 149 (2002).

39. I. Flis-Kabulska, Electrochim. Acta., **55,** 4895 (2010).

40. G. K. Pradhan and K. M. Parida, ACS. Appl Mater. Inter., **3,** 317 (2011).

41. R. Bailey and J. Castle, J. Mater. Sci., **12,** 2049 (1997).

42. O. H. Lin, H. M. Akil, and Z. A. M. Ishak, Polym. Composite., **32,** 1568 (2011).

43. E. J. Johnson, Semiconduct. Semimet., **3,** 153 (1967).

44. Y. Xu and M. A. A. Schoonen, Am. Mineral., **85,** 543 (2008).

45. J. M. Ma, J. B. Lian, X. C. Duan, X. D. Liu, and W. J. Zheng, J. Phys Chem. C., **114,** 10671 (2010).

46. R. N. Bhowmik and A. Saravanan, J. Appl Phys., **107,** 053916 (2010).

47. S. Haji, B. Benstaali, and N. Al-Bastaki, Chem. Eng. J., **168,** 134 (2011).

48. A. A. Jahagirdar, M. N. Z. Ahmed, N. Donappa, H. Nagabhushana, and B. M. Nagabhushana, T. Indian. Ceram. Soc., **70,** 159 (2011).

49. L. Obeid, A. Bee, D. Talbot, S. Ben Jaafar, V. Dupuis, S. Abramson, V. Cabuil, and M. Welschbillig, J.

Colloid Interf. Sci., **410,** 52 (2013).

Figure captions:

Figure 1. The composition and homogeneity analysis of the modified Fe_2O_3 coated PA fabric

Figure 2. FESEM images of (a) 1000× untreated, (c) 1000× and (e) 10000× modified Fe_2O_3 coated PA fiber, and (f) 30000× high-magnification FESEM image of modified Fe_2O_3 coated PA fiber; EDX spectra of (b) untreated and (d) modified Fe_2O_3 coated PA fiber

Figure 3. XRD diffractogram of the remaining particles

Figure 4. FTIR spectra of (a) untreated and (b) modified Fe_2O_3 coated PA fabrics and (c) Fe_2O_3 particles

Figure 5. TG (a) and DSC (b) curves of PA fabric before and after treatments

Figure 6. Diffuse reflectance spectra of PA fabric before and after treatments

Figure 7. Hysteresis loops of the modified Fe_2O_3 coated PA fabric and Fe_2O_3 particles at 300 K

Figure 8. Effect of irradiation time on the degradation rate of MO solution exposed to UV irradiation

Figure 1

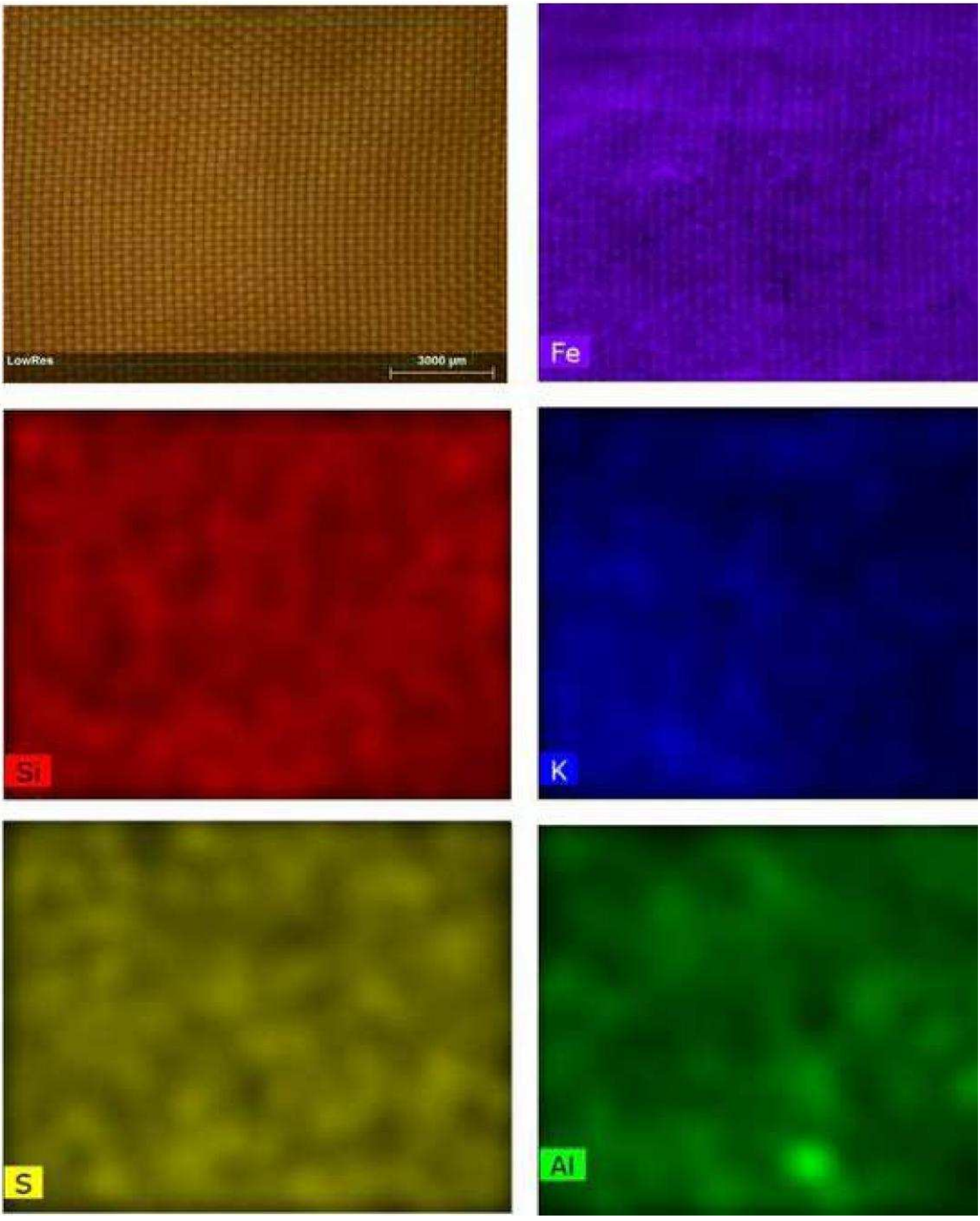

Figure 2

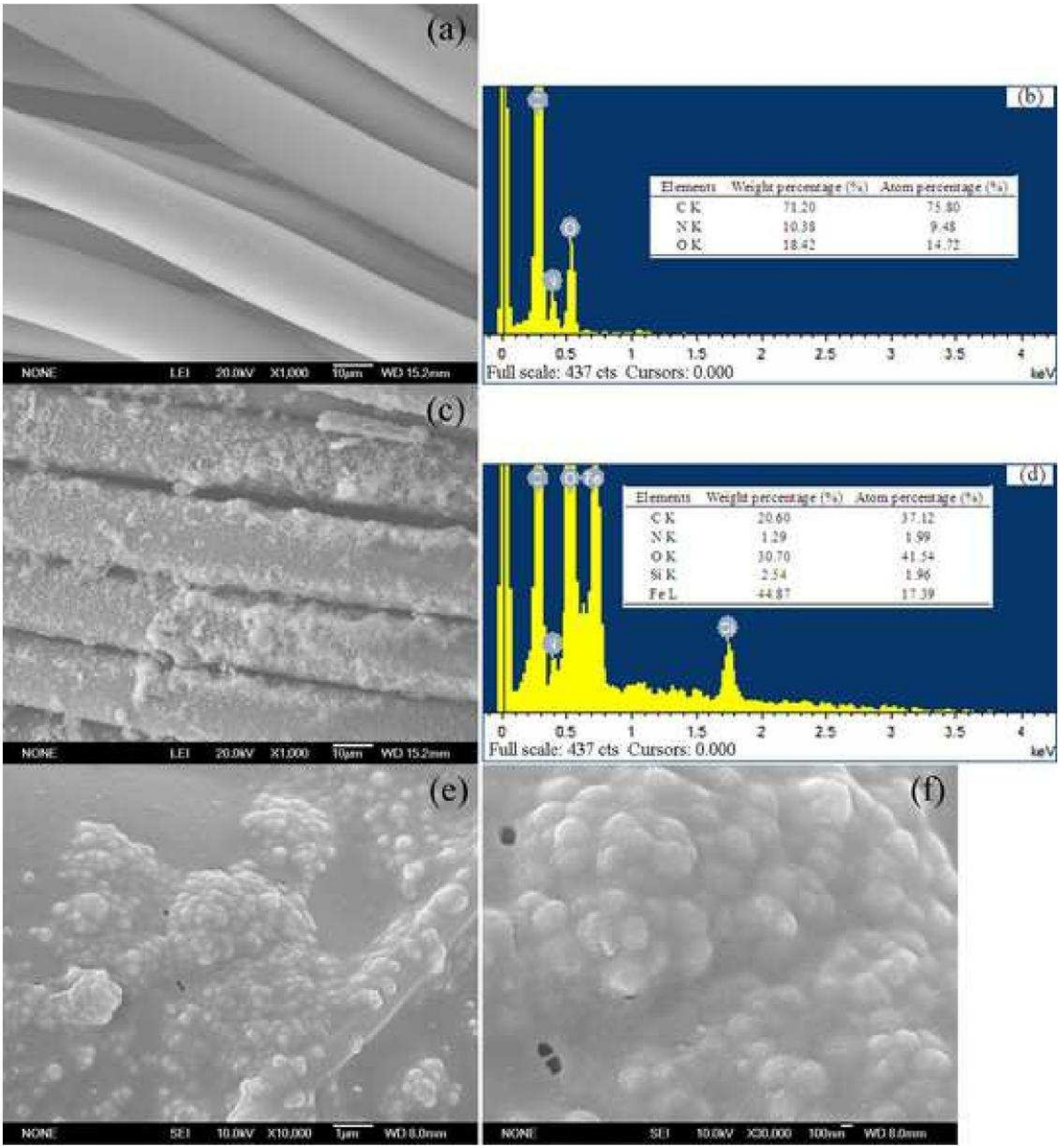
(a)
NONE LEI 20.0kV X1,000 10μm WD 15.2mm
(b)
Elements Weight percentage (%) Atom percentage (%)
C K 78.20 75.80
N K 10.38 9.48
O K 18.42 14.72
0 0.5 1 1.5 2 2.5 3 3.5 4
Full scale: 437 cts Cursors: 0.000
keV
(c)
NONE LEI 20.0kV X1,000 10μm WD 15.2mm
(d)
Elements Weight percentage (%) Atom percentage (%)
C K 20.60 37.12
N K 1.29 1.99
O K 30.70 41.54
Si K 2.54 1.96
Fe L 44.87 17.39
0 0.5 1 1.5 2 2.5 3 3.5 4
Full scale: 437 cts Cursors: 0.000
keV
(e)
NONE SEI 10.0kV X10,000 1μm WD 8.0mm
(f)
NONE SEI 10.0kV X30,000 100nm WD 8.0mm

Figure 3

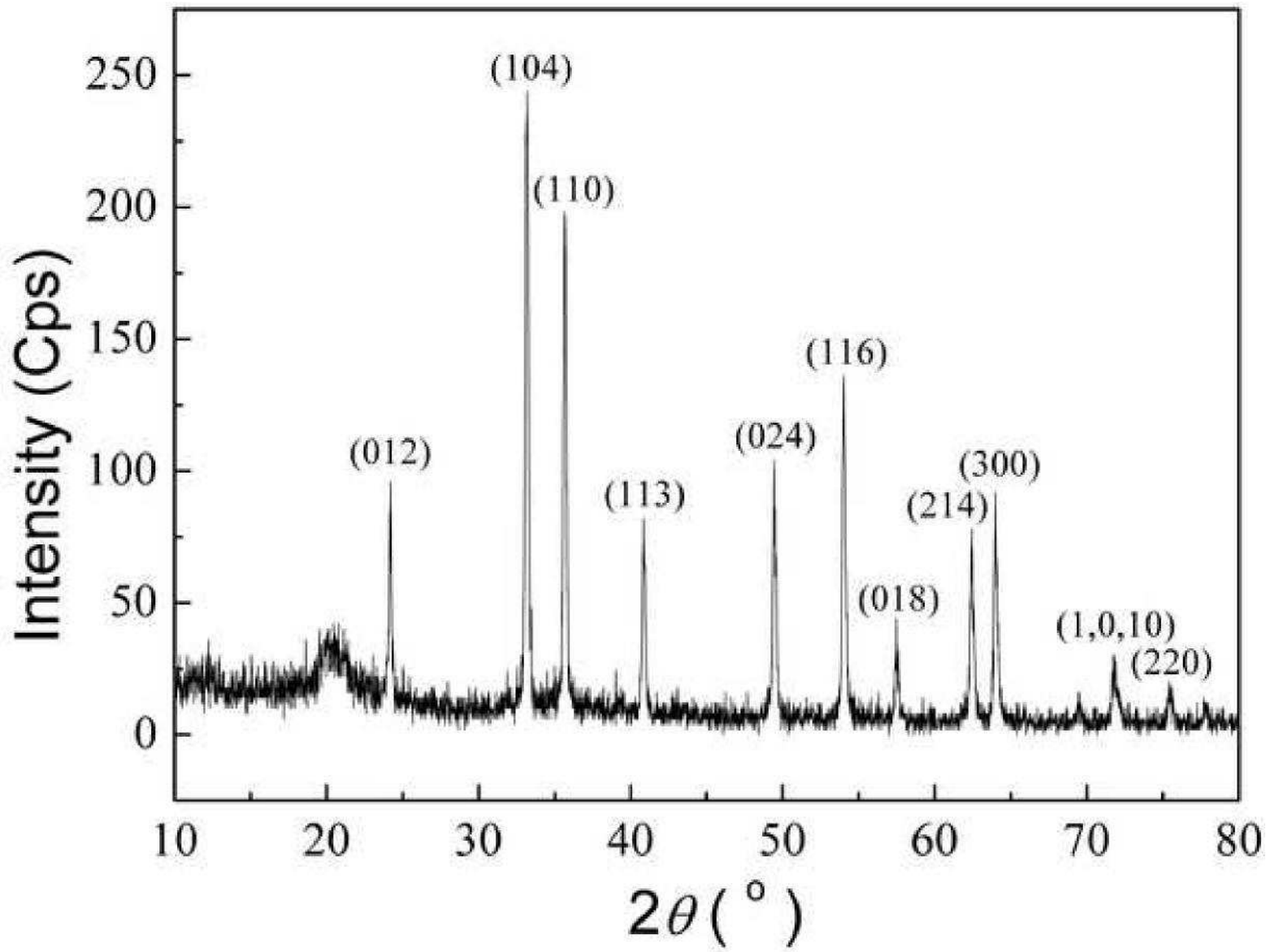
Intensity (Cps)
250
200
150
100
50
0
10
20
30
40
50
60
70
80
2θ(°)
(104)
(110)
(012)
(113)
(024)
(116)
(018)
(214)
(300)
(1,0,10)
(220)

Figure 4

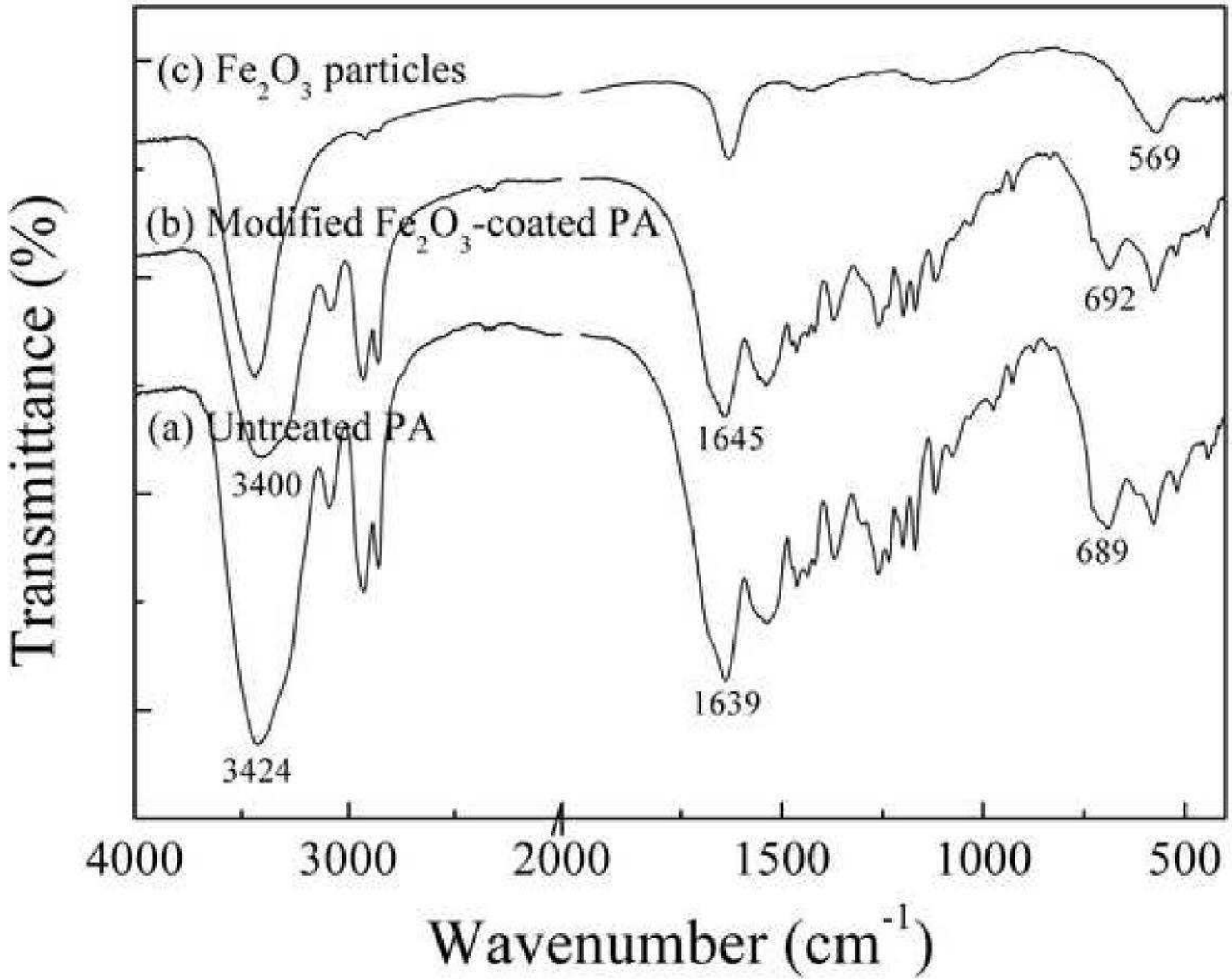
(c) Fe_2O_3 particles
(b) Modified Fe_2O_3-coated PA
(a) Untreated PA
569
692
1645
3400
689
1639
3424
Transmittance (%)
4000
3000
2000
1500
1000
500
Wavenumber (cm^{-1})

Figure 5(a)

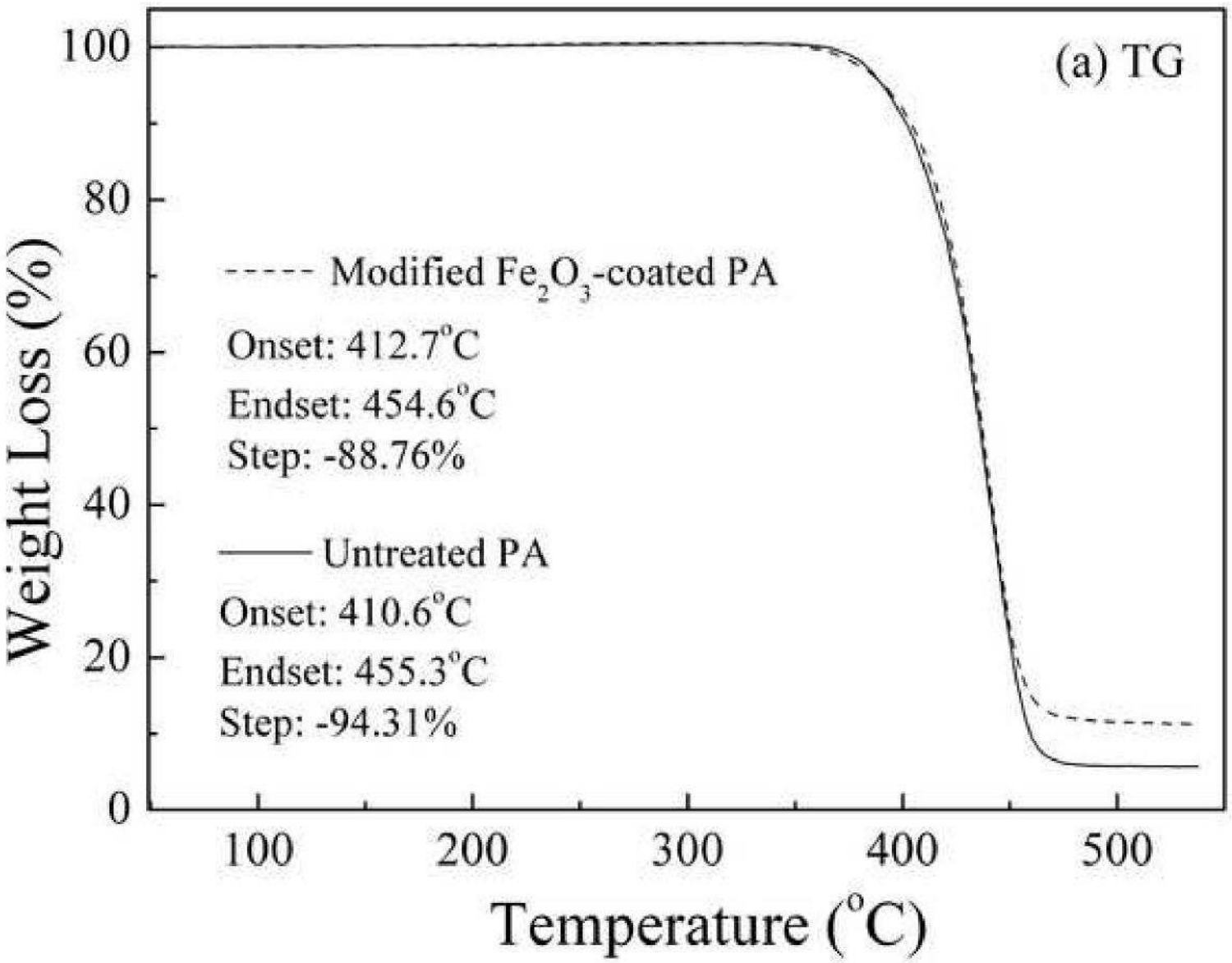
(a) TG
Weight Loss (%)
Temperature (°C)
100
80
60
40
20
0
100
200
300
400
500
----- Modified Fe2O3-coated PA
Onset: 412.7°C
Endset: 454.6°C
Step: -88.76%
—— Untreated PA
Onset: 410.6°C
Endset: 455.3°C
Step: -94.31%

Figure 5(b)

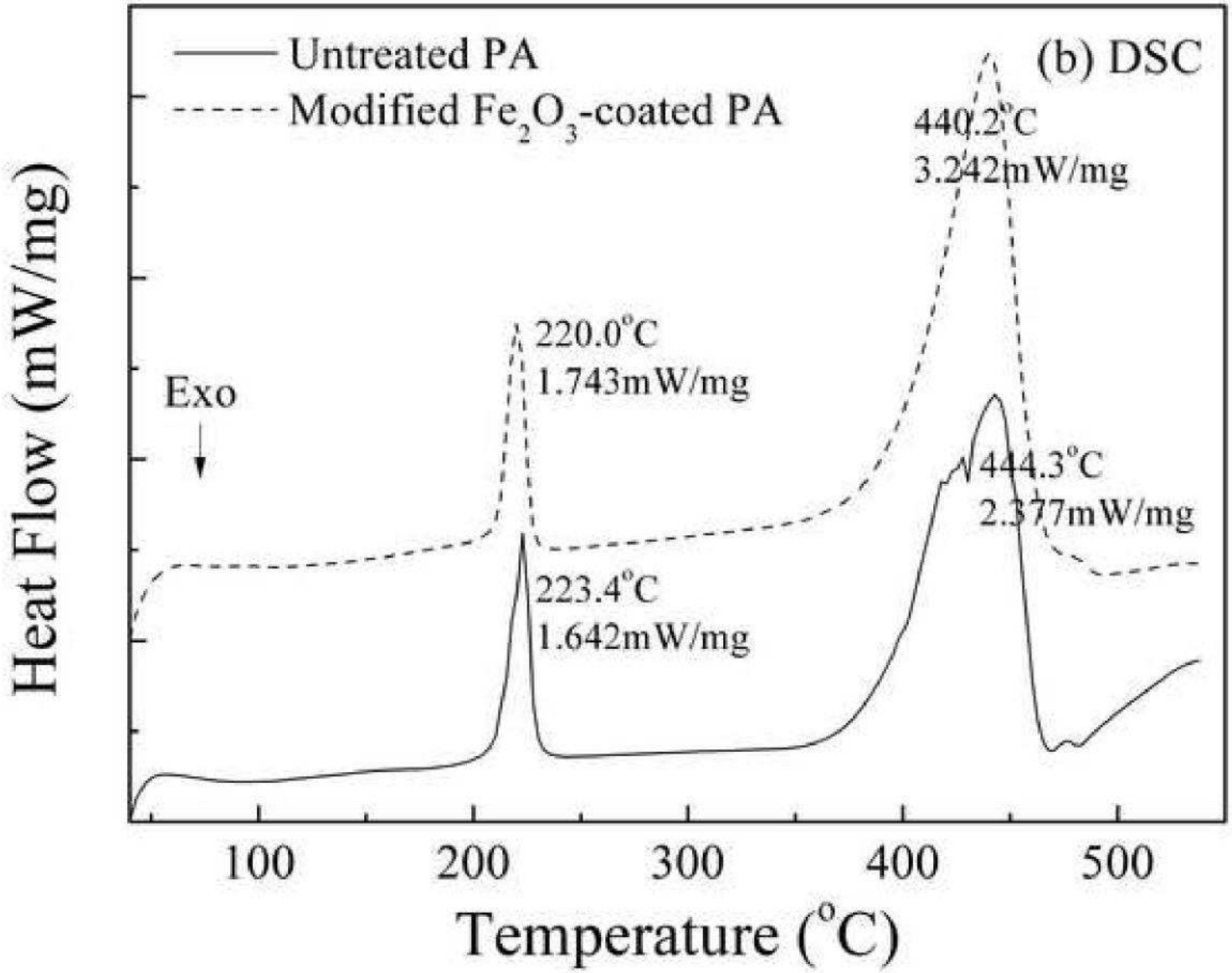
Untreated PA
Modified Fe_2O_3-coated PA
(b) DSC
440.2°C
3.242mW/mg
220.0°C
1.743mW/mg
Exo
444.3°C
2.377mW/mg
223.4°C
1.642mW/mg
Heat Flow (mW/mg)
100
200
300
400
500
Temperature (°C)

Figure 6

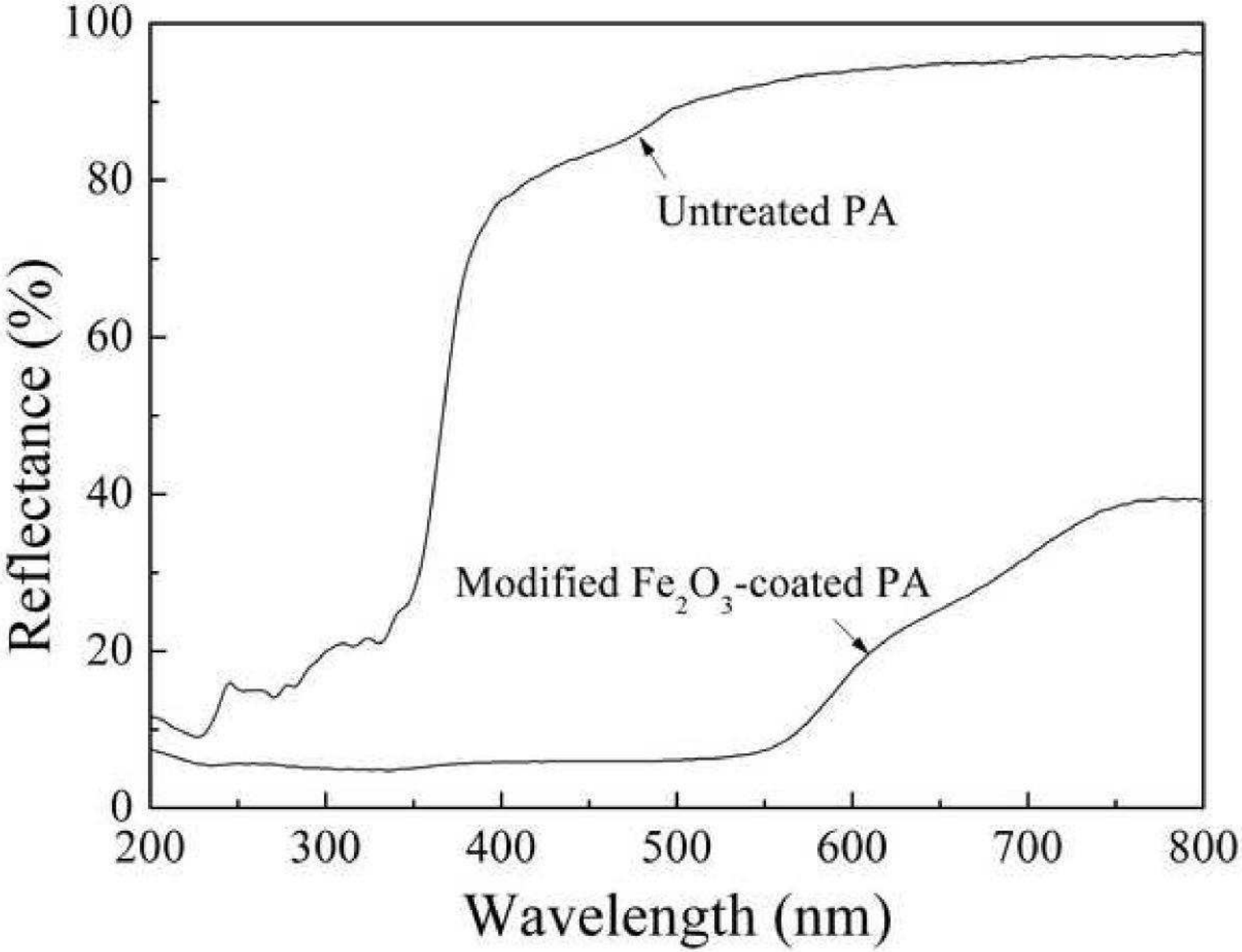
100
80
60
40
20
0
Reflectance (%)
200
300
400
500
600
700
800
Wavelength (nm)
Untreated PA
Modified Fe_2O_3-coated PA

Figure 7

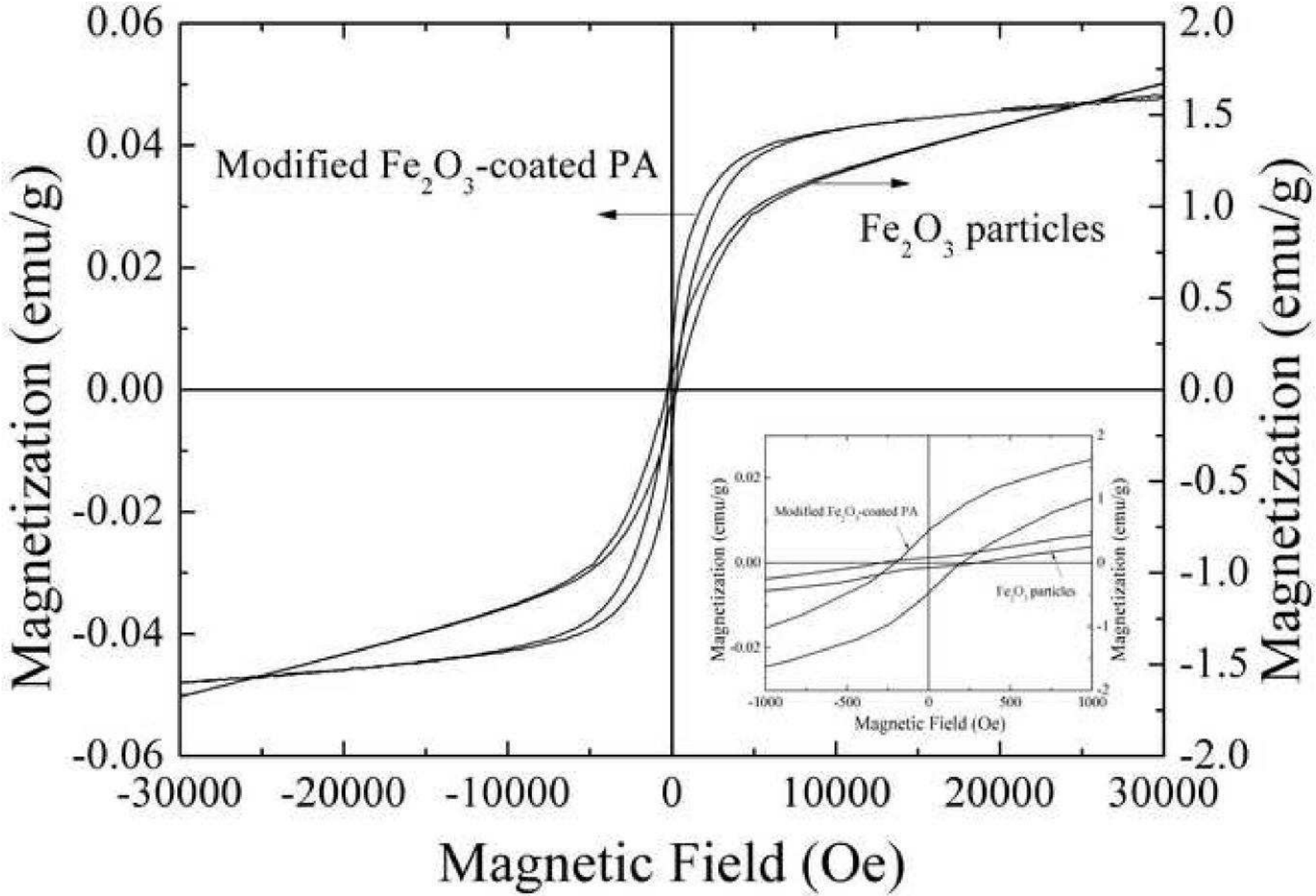
Modified Fe_2O_3-coated PA
Fe_2O_3 particles
Magnetization (emu/g)
Magnetic Field (Oe)
0.06
0.04
0.02
0.00
-0.02
-0.04
-0.06
2.0
1.5
1.0
0.5
0.0
-0.5
-1.0
-1.5
-2.0
-30000
-20000
-10000
0
10000
20000
30000
Modified Fe_2O_3-coated PA
Fe_2O_3 particles
Magnetization (emu/g)
Magnetic Field (Oe)
0.02
0.00
-0.02
2
1
0
-1
-2
-1000
-500
0
500
1000

Figure 8

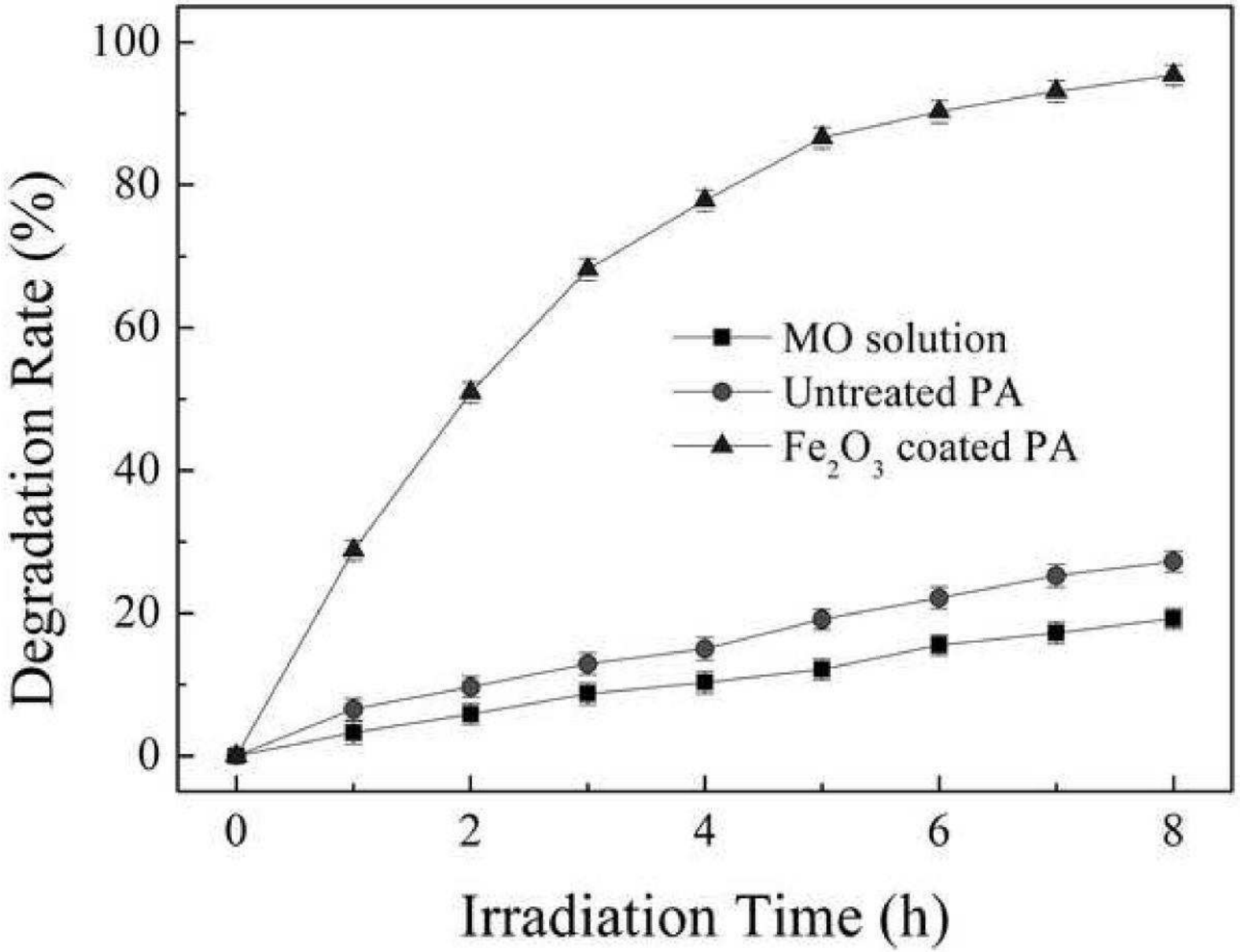
Degradation Rate (%)
100
80
60
40
20
0
0
2
4
6
8
Irradiation Time (h)
MO solution
Untreated PA
Fe2O3 coated PA